Updating the sulcal landscape of the human lateral parieto-occipital junction provides anatomical, functional, and cognitive insights

Ethan H. Willbrand[1,2*], Yi-Heng Tsai[3*], Thomas Gagnant[4], Kevin S. Weiner[1,2**]

[1]*Department of Psychology, University of California, Berkeley, Berkeley, CA, USA*
[2]*Helen Wills Neuroscience Institute, University of California, Berkeley, Berkeley, CA, USA*
[3]*Department of Psychology, University of North Carolina at Chapel Hill, Chapel Hill, NC, USA*
[4]*Medical Science Faculty, University of Bordeaux, Bordeaux, France*
**Co-first authors*
***Corresponding author:* Kevin S. Weiner (kweiner@berkeley.edu)

Abstract

Recent work has uncovered relationships between evolutionarily new small and shallow cerebral indentations, or sulci, and human behavior. Yet, this relationship remains unexplored in the lateral parietal cortex (LPC) and the lateral parieto-occipital junction (LPOJ). After defining thousands of sulci in a young adult cohort, we uncovered four previously unidentified small and shallow LPC/LOPJ sulci - one of which (ventral supralateral occipital sulcus, slocs-v) is present in nearly every hemisphere, and is morphologically, architecturally, and functionally dissociable from neighboring regions. A data-driven, model-based approach relating sulcal depth to behavior revealed that the morphology of only a subset of LPC/LPOJ sulci, including the slocs-v, is related to performance on a spatial orientation, but not a relational reasoning task. Our findings build on classic neuroanatomical theories and identify new neuroanatomical targets for future “precision imaging” studies exploring the relationship among brain structure, brain function, and cognitive abilities in individual participants.

Keywords

Cortical folding, Functional neuroanatomy, Magnetic resonance imaging (MRI), Occipital cortex, Parietal cortex, Spatial orientation

Main

A fundamental goal in psychology and neuroscience is to understand the complex relationship between brain structure and brain function, as well as how that relationship provides a scaffold for efficient cognition and behavior. Of all the neuroanatomical features to target, recent work shows that morphological features of hominoid-specific, shallow indentations, or sulci, of the cerebral cortex are not only functionally and cognitively meaningful, but also are particularly impacted by multiple brain-related disorders and aging [1–20]. The combination of these findings provides growing support for a classic theory proposing that the late emergence of these structures in gestation within association cortices, as well as their prolonged development, may co-occur with specific functional and microstructural features that could support specific cognitive abilities that also have a protracted development [21]. Nevertheless, despite the developmental, evolutionary, functional, cognitive, and theoretical relevance of these findings, they have mainly been restricted to only a subset of association cortices such as the prefrontal, cingulate, and ventral occipitotemporal cortices [1–20]. Thus, examining the relationship among these structures (also known as tertiary sulci) relative to architectonic and functional features of the cerebral cortex, as well as relative to cognition, remains uncharted in other association cortices such as the lateral parietal cortex (LPC).

As LPC is a cortical extent that has expanded extensively throughout evolution [22,23], there is great interest in the structure and function of LPC in development, aging, across species, and in different patient populations. Yet, key gaps in knowledge relating individual differences in the structure of LPC to individual differences in the functional organization of LPC and cognitive performance remain for at least four main reasons. First, one line of recent work shows that LPC displays a much more complex sulcal patterning than previously thought [24–27], while a second line of work shows that LPC is tiled with many maps and discrete functional

regions spanning modalities and functions such as vision, memory, attention, action, haptics, and multisensory integration in addition to theory of mind, cognitive control, and subdivisions of the default mode network [28–34]. Second, a majority of the time, the two lines of work are conducted independently from one another and the majority of human neuroimaging studies of LPC implement group analyses on average brain templates—which causes LPC sulci to disappear (**Fig. 1**). Third, despite the recently identified complexity of LPC sulcal patterning, recent studies have also uncovered previously overlooked tertiary sulci in association cortices (for example, in the posterior cingulate cortex [13,15]). Thus, fourth, it is unknown if additional LPC tertiary sulci are waiting to be discovered and if so, could improve our understanding of the structural-functional organization of LPC with potential cognitive insights as in other association cortices. Critically, while such findings would have developmental, evolutionary, functional, cognitive, and theoretical implications for addressing novel questions in future studies, they would also have translational applications as sulci serve as biomarkers in neurodevelopmental disorders [3–6] and “corridors” for neurosurgery [35,36].

In the present study, we first manually defined LPC sulci in 144 young adult hemispheres using the most recent definitions of LPC sulci [24]. By manually labeling over 2,000 sulci, we uncovered four previously undefined (Supplementary Methods and Supplementary Figs. 1-4 for historical details) sulci in the cortical expanse between the caudal branches of the superior temporal sulcus (cSTS) and two parts of the intraparietal sulcus (IPS)—a cortical expanse recently referenced as containing sensory “bridge” regions of the temporal-parietal-occipital junction [37]—which we term the supralateral occipital sulci (ventral: slocs-v; dorsal: slocs-d) and posterior angular sulci (ventral: pAngs-d; dorsal: pAngs-d). We then utilized morphological (depth and surface area), architectural (gray matter thickness and myelination), and functional (resting-state functional connectivity) data available in each participant to assess whether the most common of these structures (slocs-v) was dissociable from surrounding sulci. Finally, we

assessed whether the updated view of the LPC/LPOJ sulcal landscape provided cognitive insights using a model-based, data-driven approach [17] relating sulcal morphology to behavior on tasks known to activate regions within this cortical expanse (for example, reasoning and spatial orientation [38–41]).

Results

Four previously undefined small and shallow sulci in the lateral parieto-occipital junction (LPOJ)

In addition to defining the 13 sulci previously described within the LPC/LPOJ, as well as the posterior superior temporal cortex (**Methods**) [24] in individual participants, we could also identify as many as four small and shallow sulci situated within the LPC/LPOJ that were more variable across individuals and uncharted until now (Supplementary Methods and Supplementary Figs. 1-4). Macroanatomically, we could identify two sulci between the cSTS3 and the IPS-PO/ITOS ventrally and two sulci between the cSTS2 and the pips/IPS dorsally.

Ventrally, we refer to these sulci as ventral (slocs-v; sulcus 5 in **Fig. 1**) and dorsal (slocs-d; sulcus 6 in **Fig. 1**) components of the supralateral occipital sulcus. The slocs-v, located between the posterior cSTS3 and ITOS, was present in 98.6% of hemispheres (left hemisphere: N = 71/72; right hemisphere: N = 71/72; **Fig. 1**). Conversely, the slocs-d, located between the cSTS3 and IPS-PO, was present 68.0% of the time (left hemisphere: N = 50/72; right hemisphere: N = 48/72; **Fig. 1**). Dorsally, we refer to the other newly identified sulci as the ventral (pAngs-v; sulcus 7 in **Fig. 1**) and dorsal (pAngs-d; sulcus 8 in **Fig. 1**) components of the posterior angular sulcus. The pAng components were more rare than the slocs components. Specifically, pAngs-v, located between cSTS2 and pips, was identifiable 31.3% of the time (19 left and 26 right hemispheres; **Fig. 1**). Located between cSTS2 and the IPS, pAngs-d was identifiable only 13.2% of the time (8 left and 11 right hemispheres; **Fig. 1**). Though we

characterize these sulci in this paper for the first time, the location of these four sulci is consistent with the presence of variable “accessory sulci” in this cortical expanse mentioned in prior modern and classic studies (Supplementary Methods).

These incidence rates were significantly different (GLM, main effect of sulcus: $\chi 2(3) = 166.53$, $p < .0001$; no hemispheric effects: ps $> .68$). The slocs-v was more common than the other three sulci (ps $< .0001$), slocs-d was more common than the pAngs components (ps $< .0001$), and pAngs-v was more common than pAngs-d ($p = .002$). We could further identify these sulci in post-mortem hemispheres (Supplementary Figs. 2, 3). Finally, to help guide future research on these newly- and previously-classified LPC/LPOJ sulci, we generated probabilistic maps of each of these 17 sulci and share them with the field with the publication of this paper (Supplementary Fig. 6).

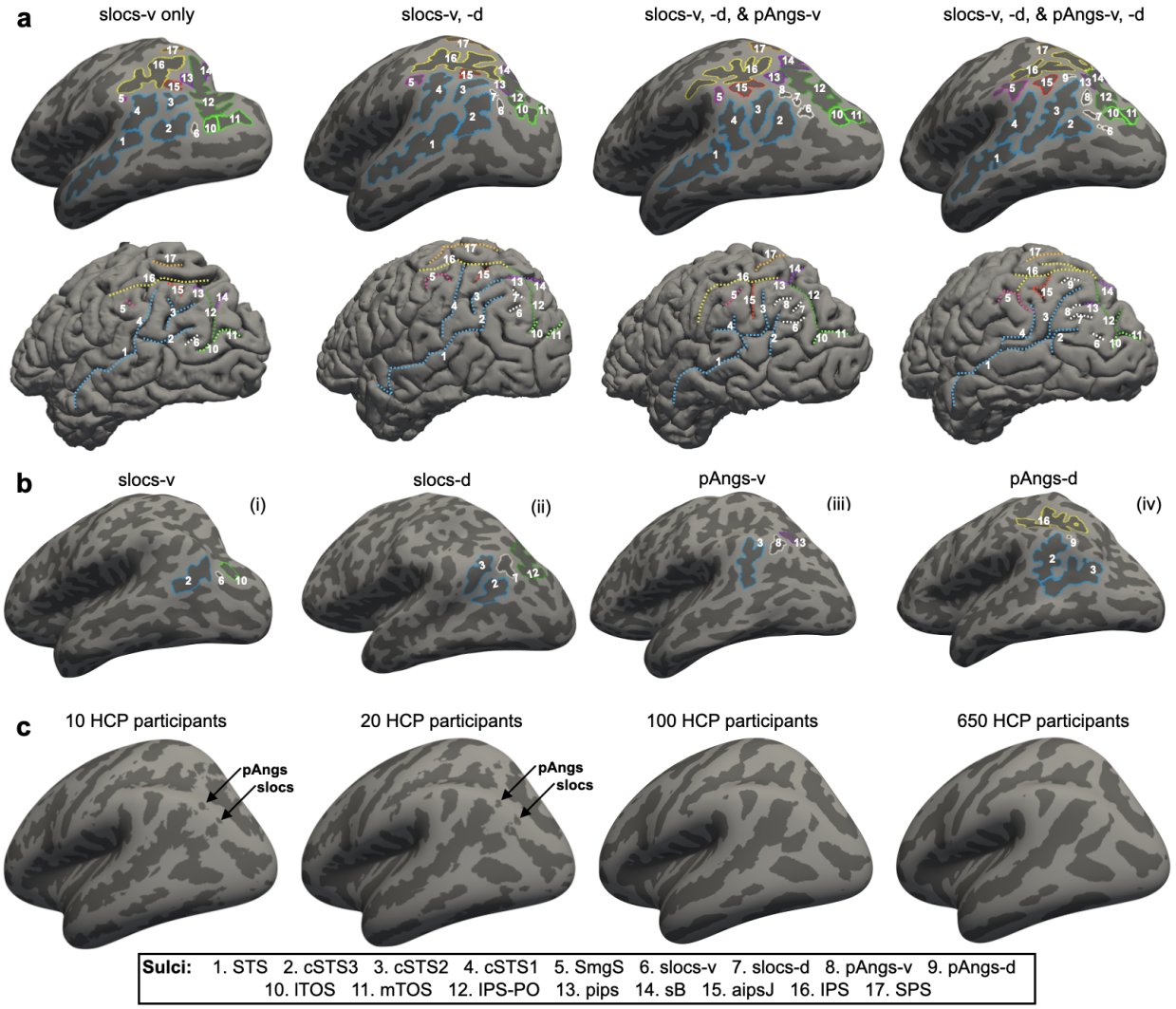

Fig. 1. Four previously undefined small and shallow sulci in the lateral parieto-occipital junction (LPOJ). a. Four example inflated (top) and pial (bottom) left hemisphere cortical surfaces displaying the 13-17 sulci manually identified in the present study. Each hemisphere contains 1-4 of the previously undefined and variable LOC/LPOJ sulci (slocs and pAngs). Each sulcus is numbered according to the legend. **b.** Criteria for defining slocs and pAngs components. (i) Slocs-v is the cortical indentation between the cSTS3 and ITOS. (ii) Slocs-d is the indentation between cSTS3/cSTS2 and IPS-PO. (iii) pAngs-v is the indentation between the cSTS2 and pips. (iv) pAngs-d is the indentation between cSTS2/cSTS1 and IPS. **c.** The variability of the slocs and pAng components can cause them to disappear when individual surfaces are averaged together. Left to right: (i) 10 HCP participants, (ii) 20 HCP participants, (iii) 100 HCP participants, and iv) 650 HCP participants. The disappearance of these sulci on average surfaces, which are often used for group analyses in neuroimaging research, emphasizes the importance of defining these structures in individual hemispheres.

The slocs-v is morphologically, architecturally, and functionally dissociable from nearby sulci

Given that the slocs-v was present in the majority of participants (98.6% across hemispheres), we focused our analyses on this stable sulcal feature of the LPOJ. To do so, we first tested whether the slocs-v was morphologically (depth and surface area) and architecturally (gray matter thickness and myelination) distinct from the two sulci surrounding it: the cSTS3 and lTOS (**Fig. 1**; Supplementary Fig. 7 for these metrics in all 17 sulci examined). An rm-ANOVA (within-participant factors: sulcus, metric, and hemisphere for standardized metric units) revealed a sulcus x metric interaction ($F(4, 276.19) = 179.15$, $\eta 2 = 0.38$, $p < .001$). Post hoc tests showed four main differences: (i) the slocs-v was shallower than cSTS3 ($p < .001$) but not lTOS ($p = .60$), (ii) the slocs-v was smaller than both the cSTS3 and lTOS (*p*s < .001), (iii) the slocs-v was thicker than both the cSTS3 and lTOS (*p*s < .001), and iv) the slocs-v was less myelinated than both the cSTS and lTOS (*p*s < .001; **Fig. 2a**). There was also a sulcus x metric x hemisphere interaction ($F(4.20, 289.81) = 4.16$, $\eta 2 = 0.01$, $p = .002$; Supplementary Results).

We then tested whether the slocs-v was also functionally distinct from the cSTS3 and lTOS by leveraging resting-state network parcellations for each individual participant to quantify "connectivity fingerprints" for each sulcus in each hemisphere of each participant (**Methods**) [42]. An rm-ANOVA (within-participant factors: sulcus, network, and hemisphere for Dice coefficient overlap) revealed a sulcus x network interaction ($F(32, 2144) = 80.18$, $\eta 2 = 0.55$, $p < .001$). Post hoc tests showed that this interaction was driven by four effects: (i) the cSTS3 overlapped more with the Default A subnetwork than both the slocs-v and lTOS (*p*s < .001), (ii) the slocs-v overlapped more with the Default C subnetwork than the lTOS ($p < .001$) and marginally than the cSTS3 ($p = .077$), (iii) the slocs-v overlapped more with the Dorsal Attention A subnetwork than both the cSTS3 and lTOS (*p*s < .001), and iv) the lTOS overlapped more with the Visual A and Visual B subnetworks than both the cSTS3 and slocs-v (*ps* < .004; **Fig. 2b**). There was also

a sulcus x network x hemisphere interaction (F(32, 2144) = 3.99, η2 = 0.06, p < .001; Supplementary Results). Together, these results indicate that the slocs-v is a morphologically, architecturally, and functionally distinct structure from its sulcal neighbors, and thus, deserves a distinct neuroanatomical definition.

We further found that the three caudal STS rami [24,25] and intermediate parietal sulci (aipsJ and pips) [24,26] are morphologically, architecturally, and functionally distinct structures for the first time (to our knowledge), which empirically supports their distinctions with separate sulcal labels (Supplementary Results and Supplementary Fig. 8).

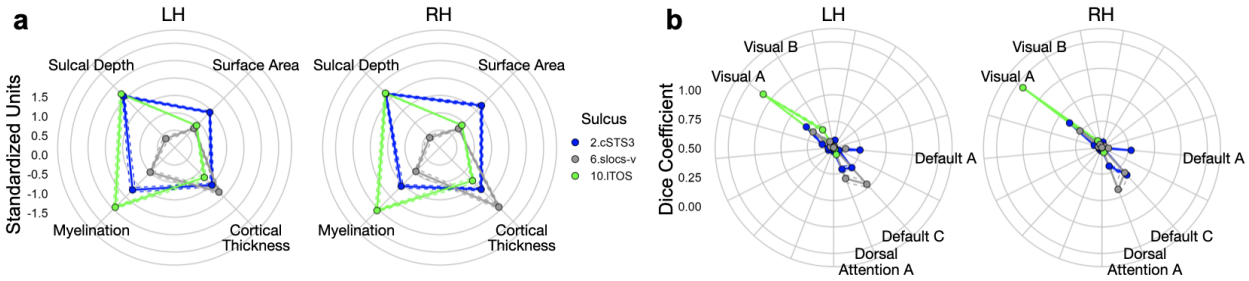

Fig. 2. The slocs-v is morphologically, architecturally, and functionally dissociable from nearby sulci. a. Radial plot displaying the morphological (upper metrics: depth, surface area) and architectural (lower metrics: cortical thickness, myelination) features of the slocs-v (gray), cSTS3 (blue), and ITOS (green). Each dot and solid line represents the mean. The dashed lines indicate ± standard error. These features are colored by sulcus (legend). Metrics are in standardized units. **b.** Radial plot displaying the connectivity fingerprints of these three sulci: the Dice Coefficient overlap (values from 0-1) between each component and individual-level functional connectivity parcellations [42].

<u>The morphology of LPC/LPOJ sulci, including the slocs-v, is related to cognitive performance</u>

Finally, leveraging a data-driven approach of cross-validated LASSO feature selection, we sought to determine whether sulcal depth, a main defining feature of sulci, related to cognitive performance (**Methods**). To do so, we primarily focused on spatial orientation and reasoning given that these abilities recruit multiple subregions of lateral parietal and/or occipital cortices

[38–41]. As in prior work [16–18], we chose the model at the alpha that minimized MSE_{cv}. Participants with a slocs-v in both hemispheres and all behavioral metrics were included (N = 69). Due to their rarity (being in less than 70% of hemispheres at most), we did not include the slocs-d or pAng components in this analysis.

This method revealed an association between spatial orientation scores and normalized sulcal depth in the left hemisphere (MSE_{cv} = 25.63, alpha = 0.05; **Fig. 3a**), but not in the right hemisphere (MSE_{cv} = 26.41, alpha = 0.3). Further, we found that no LPC/LPOJ sulci were selected for reasoning in either hemisphere (right*:* alpha = 0.3, MSE = 24.01; left: alpha = 0.3, MSE = 24.01). Six left hemisphere LPC/LPOJ sulci were related to spatial orientation task performance **Fig. 3a, b**). Four of these sulci were positioned ventrally: cSTS3 (β = -9.77), slocs-v (β = -3.36), lTOS (β = -4.91), and mTOS (β = -0.06), whereas two were positioned dorsally: pips (β = 5.02), and SPS (β = 4.30; **Fig. 3a, b**). Using LooCV to construct models that predict behavior, the LASSO-selected model explained variation in spatial orientation score (R^2_{cv} = 0.06, MSE_{cv} = 23.99) above and beyond a model with all left hemisphere sulci (R^2_{cv} < 0.01, MSE_{cv} = 27.12). This model also showed a moderate correspondence (r_s = 0.29, p = .01; **Fig. 3c**) between predicted and actual measured scores. We then tested for anatomical and behavioral specificity using the AIC, which revealed two primary findings. First, we found that the LASSO-selected sulcal depth model outperformed a model using the cortical thickness of the six LASSO-selected sulci (R^2_{cv} < .01, MSE_{cv} = 26.02, $AIC_{cortical\ thickness} – AIC_{sulcal\ depth}$ = 2.19). This model also showed task specificity as these sulci outperformed a model with processing speed (R^2_{cv} < .01, MSE_{cv} = 254.65, $AIC_{processing\ speed} – AIC_{spatial\ orientation}$ = 63.57). Thus, our data-driven model explains a significant amount of variance on a spatial orientation task and shows behavioral and morphological specificity.

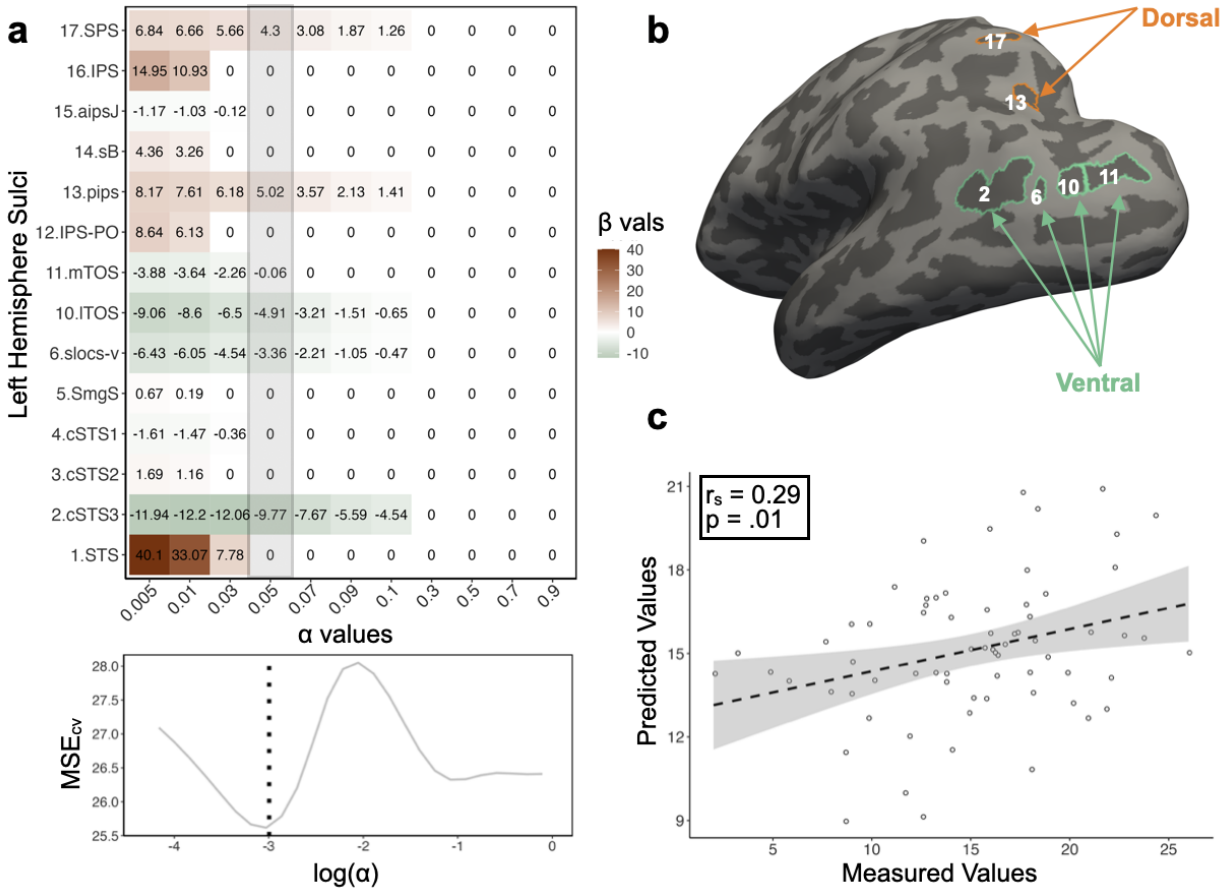

Fig. 3. The morphology of LPC/LPOJ sulci, including the slocs-v, is related to cognitive performance. a. Beta-coefficients for each left hemisphere LPC/LPOJ sulcus at a range of shrinking parameter values [alpha (α)]. Highlighted gray bar indicates coefficients at the chosen α-level. Bottom: Cross-validated mean-squared error (MSE_{CV}) at each α level. By convention, we selected the α that minimized the MSE_{CV} (dotted line). **b.** Inflated left hemisphere cortical surface from an example participant highlighting the two groups of sulci—*dorsal positive* (orange) and *ventral negative* (green)—related to spatial orientation performance. **c.** Spearman's correlation (r_s) between the measured and the predicted spatial orientation scores from the LASSO-selected model is shown in a.

Discussion

<u>Overview</u>

In the present study, we examined the relationship between LPC/LPOJ sulcal morphology, functional connectivity fingerprints, and cognition. We report five main findings. First, while manually defining sulci in LPC/LPOJ across 144 hemispheres, we uncovered four new small and shallow sulci that are not included in present or classic neuroanatomy atlases or

neuroimaging software packages. Second, we found that the most common of these structures (the slocs-v; identifiable 98.6% of the time) was morphologically, architecturally, and functionally differentiable from nearby sulci. Third, using a model-based, data-driven approach quantifying the relationship between sulcal morphology and cognition, we found a relationship between the depths of six LPC/LPOJ sulci and performance on a spatial orientation processing task. Fourth, the model identified distinct dorsal and ventral sulcal networks in LPC/LPOJ: ventral sulci had negative weights while dorsal sulci had positive weights (**Fig. 3b**). These findings are consistent with previous neuroimaging work from Gur et al. [41] who demonstrated separate functional activations in dorsal parietal and the more ventrally situated occipital-parietal cortices for the judgment of line orientation task used in the present study. Fifth, the model identified that the slocs-v is cognitively relevant, further indicating the importance of this new neuroanatomical structure. In the sections below, we discuss (i) the slocs-v relative to modern functional and cytoarchitectonic parcellations in the LPC/LPOJ, as well as anatomical connectivity to other parts of the brain, (ii) underlying anatomical mechanisms relating sulcal morphology and behavior more broadly, and (iii) limitations of the present study. Implications for future studies are distributed throughout each section.

The slocs-v relative to modern functional and cytoarchitectonic parcellations in the LPC/LPOJ, as well as anatomical connectivity to other parts of the brain

To lay the foundation for future studies relating the newly-identified slocs-v to different anatomical and functional organizational features of LPC/LPOJ, we situate probabilistic predictions of slocs-v relative to probabilistic cortical areas identified using multiple modalities. For example, when examining the correspondence between the slocs-v and modern multimodal (HCP-MMP [37]) and observer-independent cytoarchitectural (Julich-Brain atlas [43]) areas (Methods), the slocs-v is located within distinct areas. In particular, the slocs-v aligns with the

multimodally- and cytoarchitecturally-defined area PGp bilaterally and cytoarchitecturally-defined hIP4 in the right hemisphere (**Fig. 4**). In classic neuroanatomical terms [44], this indicates that the slocs-v is a putative "axial sulcus" for these regions, which future work can assess with analyses in individual participants.

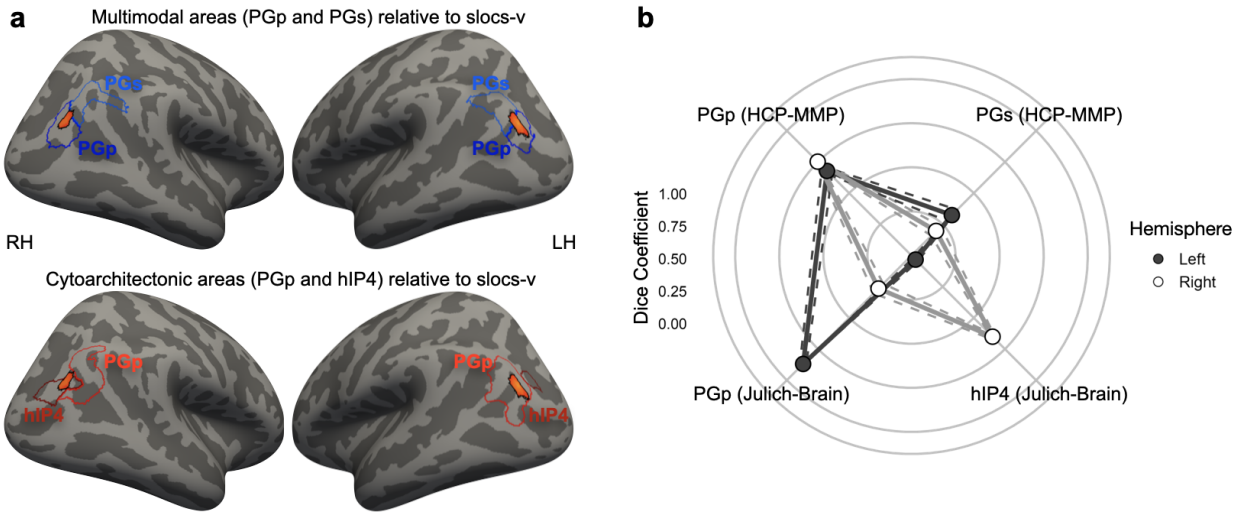

Fig. 4. The slocs-v relative to modern functional and cytoarchitectonic parcellations in LPC/LPOJ. a. Top: Left (LH) and right (RH) hemispheres of the inflated fsaverage surface with two areas from the modern HCP multimodal parcellation (HCP-MMP; blue) [37] relative to an MPM of the slocs-v (warm colors indicate areas with at least 20% overlap across participants; Supplementary Fig. 6). Bottom: Same as top, except for two observer-independent cytoarchitectonic regions from the Julich-Brain Atlas [43]. **b.** Overlap between the slocs-v and each area (Methods). Each dot and solid line represents the mean. The dashed lines indicate ± standard error (left: gray; right: white).

Aside from recent multimodal and observer-independent cytoarchitectonic parcellations, an immediate question is: What is the relationship between the slocs-v and other functional regions at this junction between the occipital and parietal lobes, as well as potential anatomical connectivity? For example, there are over a dozen visual field maps in the cortical expanse spanning the TOS, IPS-PO, and the IPS proper (see (i), (ii), and (iii), respectively in **Fig. 5a**) [33]. When projecting probabilistic locations of retinotopic maps from over 50 individuals from Wang and colleagues [45] (Methods), the slocs-v is likely located outside of visual field maps extending

into this cortical expanse (**Fig. 5a**). Nevertheless, when also projecting the map of the mean R^2 metric from the HCP retinotopy dataset from 181 participants shared by Benson and colleagues [46] (Methods), the slocs-v is in a cortical expanse that explains a significant amount of variance (left hemisphere: R^2_{mean} = 19.29, R^2_{max} = 41.73; right hemisphere: R^2_{mean} = 21.17, R^2_{max} = 44.23; **Fig. 5b**).

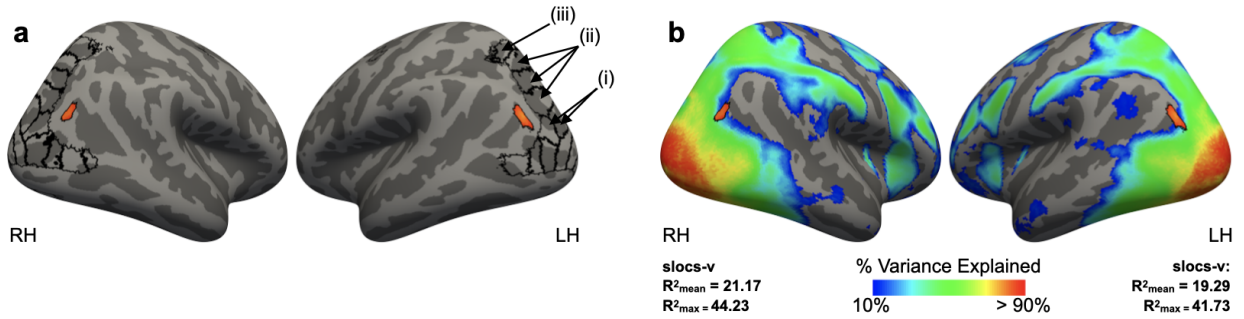

Fig. 5. The slocs-v relative to retinotopy. a. Top: Left (LH) and right (RH) hemispheres of the inflated fsaverage surface displaying the probabilistic locations of retinotopic maps from over 50 individuals from Wang and colleagues [45] (black outlines). The predicted slocs-v location from the MPMs is overlaid in orange (as in Fig. 4). (i), (ii), and (iii) point out the retinotopic maps in the cortical expanse spanning the TOS, IPS-PO, and IPS, respectively. **b.** Same format as in a, but with a map of the mean R^2 metric from the HCP retinotopy dataset [46] overlayed on the fsaverage surfaces (thresholded between R^2 values of 10% and 90%). This metric measures how well the fMRI time series at each vertex is explained by a population receptive field (pRF) model. The mean and max R^2 values for the slocs-v MPM in each hemisphere are included below each surface.

In terms of anatomical connectivity, as the slocs-v co-localizes with cytoarchitectonically defined PGp (**Fig. 4**) and previous studies have examined the anatomical connectivity of the probabilistically defined PGp, we can glean insight regarding the anatomical connectivity of slocs-v from these previous studies [47,48]. This prior work showed that PGp was anatomically connected to temporo-occipital regions, other regions in the temporal lobe, middle and superior frontal cortex, as well as the inferior frontal cortex and insula [47,48]. Furthermore, the slocs-v appears to lie at the junction of scene-perception and place-memory activity (a transition that also consistently co-localizes with the HCP-MMP area PGp) as identified by Steel and

colleagues[49]. Of course, the location of the slocs-v relative to multimodal, cytoarchitectonic, and retinotopic areas, as well as the anatomical connectivity of the slocs-v, would need to be examined in individual participants, but the present work makes clear predictions for future studies as fleshed out here. To conclude this section, as the multimodal area PGp (**Fig. 4**) was recently proposed as a "transitional area" by Glasser and colleagues [37] (Supplementary Table 1), future studies can also further functionally and anatomically test the transitional properties of slocs-v.

Underlying anatomical mechanisms relating sulcal morphology and behavior

In this section, we discuss potential anatomical mechanisms contributing to the relationship between sulcal depth and behavior in two main ways. First, long-range white matter fibers have a gyral bias, while short-range white matter fibers have a sulcal bias in which some fibers project directly from the deepest points of a sulcus [50–54]. As such, recent work hypothesized a close link between sulcal depth and short-range white matter properties [16–18,55,56]: deeper sulci would reflect even shorter short-range white matter fibers, which would result in faster communication between local, cortical regions and in turn, contribute to improved cognitive performance. This increased neural efficiency could underlie individual differences in cognitive performance. Ongoing work is testing this hypothesis which can be further explored in future studies incorporating anatomical, functional, and behavioral measures, as well as computational modeling.

Second, our model-based approach identified separate dorsal and ventral sulcal networks in which deeper sulci dorsally and shallower sulci ventrally contributed to the most explained variance on the spatial orientation task. A similar finding was identified by our previous work in the lateral prefrontal cortex [18]. These previous and present findings may be explained by the classic anatomical compensation theory, which proposes that the size and

depth of a sulcus counterbalance those of the neighboring sulci [23,57,58]. Thus, a larger, deeper sulcus would be surrounded by sulci that are smaller and shallower, rendering the overall degree of cortical folding within a given region approximately equal [23,57,58]. Future work can incorporate underlying white matter architecture into the compensation theory, as well as a recent modification that proposed to also incorporate local morphological features such as the deepest sulcal point (e.g., sulcal pit or sulcal root [59]), which has recently been shown to be related to different functional features of the cerebral cortex [60–62]. Altogether, these and recent findings begin to build a multimodal mechanistic neuroanatomical understanding underlying the complex relationship between sulcal depth and cognition relative to other anatomical features.

Limitations

The main limitation of our study is that presently, the most accurate methodology to define sulci —especially the small, shallow, and variable tertiary sulci—requires researchers to manually trace each structure on the cortical surface reconstructions. This method is arduous and time-consuming, which, on the one hand, limits the sample size in terms of number of participants, while on the other, results in thousands of precisely defined sulci - a push-pull relationship reflecting a conversation in the broader human brain mapping and cognitive neuroscience fields between a balance of large N studies and “precision imaging” studies in individual participants [63–66]. Though our sample size is comparable to other studies that produced reliable results relating sulcal morphology to brain function and cognition (e.g., [3,4,8,10,12,13,17–19,67]), ongoing work that uses deep learning algorithms to automatically define sulci should result in much larger sample sizes in future studies [68,69]. Finally, the time-consuming manual definitions of primary, secondary, and tertiary sulci also limit the cortical expanse explored in each study, thus, restricting the present study to LPC/LPOJ.

Conclusion

In conclusion, we uncovered four previously-undefined sulci in LPC/LPOJ and quantitatively showed that the slocs-v is a stable sulcal landmark that is morphologically, architecturally, and functionally differentiable from surrounding sulci. We further used a data-driven, model-based approach relating sulcal morphology to behavior, which identified different relationships of ventral and dorsal LPC/LPOJ sulcal networks contributing to the perception of spatial orientation. The model identified the slocs-v, further indicating the importance of this new neuroanatomical structure. Altogether, this work provides a scaffolding for future “precision imaging” studies interested in understanding how anatomical and functional features of LPC/LPOJ relate to cognitive performance at the individual level.

Methods

Participants

Data for the young adult human cohort analyzed in the present study were from the Human Connectome Project (HCP) database (https://www.humanconnectome.org/study/hcp-young-adult/overview). Here, we used 72 participants (50% female, 22-36 years old, and 90% right-handed; there was no effect of handedness on our behavioral tasks; Supplementary materials) that were also analyzed in several prior studies [11–16]. HCP consortium data were previously acquired using protocols approved by the Washington University Institutional Review Board (Mapping the Human Connectome: Structure, Function, and Heritability; IRB # 201204036). Informed consent was obtained from all participants.

Neuroimaging data acquisition

Anatomical T1-weighted (T1-w) MRI scans (0.8 mm voxel resolution) were obtained in native space from the HCP database. Reconstructions of the cortical surfaces of each participant were generated using FreeSurfer (v6.0.0), a software package used for processing and analyzing human brain MRI images (surfer.nmr.mgh.harvard.edu) [70,71]. All subsequent sulcal labeling and extraction of anatomical metrics were calculated from these reconstructions generated through the HCP's version of the FreeSurfer pipeline [72].

Behavioral data

In addition to structural and functional neuroimaging data, the HCP also includes a wide range of behavioral metrics from the NIH toolbox [73]. To relate LPC/LPOJ sulcal morphology to behavior, we leveraged behavioral data related to spatial orientation (Variable Short Penn Line Orientation Test), relational reasoning (Penn Progressive Matrices Test), and processing speed

(Pattern Completion Processing Speed Test; Supplementary Methods for task details). We selected these tasks as previous functional neuroimaging studies have shown the crucial role of LPC/LPOJ in relational reasoning and spatial orientation [38–41], while our previous work relating sulcal morphology to cognition uses processing speed performance as a control behavioral task [17,19].

Anatomical analyses

Manual labeling of LPC sulci

Sulci were manually defined in 72 participants (144 hemispheres) guided by the most recent atlas by Petrides [24], as well as recent empirical studies [25–27], which together offer a comprehensive definition of cerebral sulcal patterns, including tertiary sulci. For a historical analysis of sulci in this cortical expanse, please refer to Segal & Petrides [25] and Zlatkina & Petrides [26]. Our cortical expanse of interest was bounded by the following sulci and gyri: (i) the postcentral sulcus (PoCS) served as the anterior boundary, (ii) the superior temporal sulcus (STS) served as the inferior boundary, (iii) the superior parietal lobule (SPL) served as the superior boundary, and (iv) the medial and lateral transverse occipital sulci (mTOS and lTOS) served as the posterior boundary. We also considered the following sulci within this cortical expanse: the three different branches of the caudal superior temporal sulcus (posterior to anterior: cSTS3, 2, 1), the supramarginal sulcus (SmgS), posterior intermediate parietal sulcus (pips), sulcus of Brissaud (sB), anterior intermediate parietal sulcus of Jensen (aipsJ), paroccipital intraparietal sulcus (IPS-PO), intraparietal sulcus (IPS), and the superior parietal sulcus (SPS). Of note, the IPS-PO is the portion of the IPS extending ventrally into the occipital lobe. The IPS-PO was first identified as the paroccipital sulcus by Wilder (1886). There is often an annectant gyrus separating the horizontal portion of the IPS proper from the IPS-PO [26,67].

Additionally, we identified as many as four previously uncharted and variable tertiary LPC/LPOJ sulci for the first time: the supralateral occipital sulcus (slocs; composed of ventral (slocs-v) and dorsal (slocs-d) components) and the posterior angular sulcus (pAngs; composed of ventral (pAngs-v) and dorsal (pAngs-d) components). In the Supplementary Methods and Supplementary Figs. 1-4, we discuss the slocs and pAngs within the context of modern and historical sources.

For each participant in each hemisphere, the location of each sulcus was confirmed by trained independent raters (E.H.W., Y.T., and T.G.) and finalized by a neuroanatomist (K.S.W.). All LPC sulci were then manually defined in FreeSurfer using tksurfer tools, as in previous work [11–20], from which morphological and anatomical features were extracted. For four example hemispheres with these 13-17 sulci identified, see **Fig. 1a** (Supplementary Fig. 5 for all hemispheres). The specific criteria to identify the slocs and pAngs are outlined in **Fig. 1b**.

To test whether the incidence rates of the slocs and pAngs components were statistically different, we implemented a binomial logistic regression GLM with sulcus (slocs-v, slocs-d, pAngs-v, and pAngs-d) and hemisphere (left and right), as well as their interaction, as predictors for sulcal presence [0 (absent), 1 (present)]. GLMs were carried out with the glm function from the built-in stats R package. ANOVA $\chi 2$ tests were applied to each GLM with the Anova function from the car R package, from which results were reported.

Probability maps

Sulcal probability maps were generated to show the vertices with the highest alignment across participants for a given sulcus. To create these maps, the label file for each sulcus was transformed from the individual to the fsaverage surface with the FreeSurfer mri_label2label command (https://surfer.nmr.mgh.harvard.edu/fswiki/mri_label2label). Once each label was transformed into this common template space, we calculated the proportion of participants for

which each vertex was labeled as the given sulcus with custom Python code [12,17]. For vertices with overlap between sulci, we employed a "winner-take-all" approach such that the sulcus with the highest overlap across participants was assigned to that vertex. Alongside the thresholded maps, we also provide constrained maps [maximum probability maps (MPMs)] at 20% participant overlap to increase interpretability (20% MPMs shown in Supplementary Fig. 6). To aid future studies interested in investigating LPC/LPOJ sulci, we share these maps with the field.

Extracting and comparing the morphological and architectural features from sulcal labels

Morphologically, we compared sulcal depth and surface area across sulci, as these are two of the primary morphological features used to define and characterize sulci [8,10–13,16–18,21,58,60,62,74,75]. As in our prior work [17,18], mean sulcal depth values (in standard FreeSurfer units) were computed in native space from the .sulc file generated in FreeSurfer [70] with custom Python code [17]. Briefly, depth values are calculated based on how far removed a vertex is from what is referred to as a "mid-surface," which is determined computationally so that the mean of the displacements around this "mid-surface" is zero. Thus, generally, gyri have negative values, while sulci have positive values. Each depth value was also normalized by the deepest point in the given hemisphere. Surface area (mm^2) was calculated with the FreeSurfer mris_anatomical_stats function (https://surfer.nmr.mgh.harvard.edu/fswiki/mris_anatomical_stats). The morphological features of all LPC/LPOJ sulci are documented in Supplementary Fig. 7.

Architecturally, we compared cortical thickness and myelination, as in our prior work in other cortical expanses [12,13,16,17]. Mean gray matter cortical thickness (mm) was extracted using the FreeSurfer mris_anatomical_stats function. To quantify myelin content, we used the T1-w/T2-w maps for each hemisphere, an in vivo myelination proxy [76]. To generate the

T1-w/T2-w maps, two T1-w and T2-w structural MR scans from each participant were registered together and averaged as part of the HCP processing pipeline [72]. The averaging helps to reduce motion-related effects or blurring. Additionally, and as described by Glasser and colleagues [72], the T1-w/T2-w images were bias-corrected for distortion effects using field maps. We then extracted the average T1-w/T2-w ratio values across each vertex for each sulcus using custom Python code [12]. The architectural features of all LPC/LPOJ sulci are documented in Supplementary Fig. 7.

To assess whether these four metrics differed between the slocs-v and surrounding sulci (cSTS3 and ITOS), we ran a repeated measure analysis of variance (rm-ANOVA) with the within-participant effects of sulcus (slocs-v, cSTS3, and ITOS), metric (surface area, depth, cortical thickness, and myelination), and hemisphere (left and right). Rm-ANOVAs (including sphericity correction) were implemented with the aov_ez function from the afex R package. Effect sizes for the ANOVAs are reported with the partial eta-squared metric (η2). Post-hoc analyses were computed with the emmeans function from the emmeans R package (*p*-values corrected with Tukey's method). We also repeated these analyses for the three cSTS components [24,25] and the two intermediate parietal sulcal components (ips: aipsJ and pips [24,26]; detailed in the Supplementary Results and Supplementary Fig. 8) as these components, to our knowledge, have not been quantitatively compared in previous work.

Functional analyses

To determine if the slocs-v is functionally distinct from surrounding sulci, we generated functional connectivity profiles using recently developed analyses [12,13,77]. First, we used resting-state network parcellations for each individual participant from Kong and colleagues [42], who generated individual network definitions by applying a hierarchical Bayesian network algorithm to produce maps for each of the 17 networks in individual HCP participants. Importantly, this parcellation

was conducted blind to both cortical folding and our sulcal definitions. Next, we resampled the network profiles for each participant onto the fsaverage cortical surface, and then to each native surface using CBIG tools (https://github.com/ThomasYeoLab/CBIG). We then calculated the spatial overlap between a sulcus and each of the 17 individual resting-state networks via the Dice coefficient (Equation 1):

$$(1)\ \ DICE\,(X,Y) \ = \ \frac{2\,|X \cap Y|}{|X| + |Y|}$$

This process of calculating the overlap between each sulcus and the 17-network parcellation generated a “connectivity fingerprint” for each sulcus in each hemisphere of each participant. We then ran an rm-ANOVA with within-participant factors of sulcus (slocs-v, cSTS3, and ITOS), network (17 networks), and hemisphere (left and right) to determine if the network profiles (i.e., the Dice coefficient overlap with each network) of the slocs-v was differentiable from the surrounding sulci (i.e., cSTS3 and ITOS). Here we discuss effects related to networks that at least showed minor overlap with one sulcus (i.e., Dice ≥ .10). As in the prior analysis, we also repeated these analyses for the three cSTS components and the two intermediate parietal sulcal components (Supplementary Results and Supplementary Fig. 8).

Behavioral analyses

Model selection

The analysis relating sulcal morphology to spatial orientation and/or reasoning consisted of using a cross-validated least absolute shrinkage and selection operator (LASSO) regression to select the sulci that explained the most variance in the data and determined how much variance is explained by sulcal depth as a predictor of behavior, as implemented in our previous work [16–18]. The depths of all LPC/LPOJ sulci were included as predictors in the LASSO regression model (Supplementary Methods for details on demographic control variables). As the shrinkage parameter (alpha) increases, it decreases the coefficient of each of the sulci to zero except for

those with the strongest association. Therefore, this technique highlights the sulci whose morphology was most closely related to behavior. We used cross-validation to optimize the shrinking parameter for the LASSO regression. Conventionally, we selected the model parameters that minimized the cross-validated mean squared error (MSE_{cv}) [78]. The optimization was performed with the GridSearchCV function sklearn in Python, which allowed us to determine the model parameters minimizing the MSE_{cv}. To evaluate the performance of any model selected by the LASSO regression, as in prior work [16–18], we measured the model performance for the relevant behavioral task using nested model comparison. With leave-one-out cross-validation (LooCV), we compared the LASSO-selected model with the predictors to a model with all left hemisphere sulci as predictors.

Assessing morphological and behavioral specificity

To assess whether our findings generalized to other anatomical features, we considered cortical thickness, which is consistently studied in cognitive neuroscience studies relating morphology to cognition [16–18,79,80]. To do so, we replaced sulcal depth with cortical thickness as the predictive metric in our LASSO-selected model. As with depth, the model was fit to the data with LooCV. To compare the thickness model to the depth model, we used the Akaike Information Criterion (AIC), which provides an estimate of in-sample prediction error and is suitable for non-nested model comparison. By comparing AIC scores, we are able to assess the relative performance of the two models. If the ΔAIC is > 2, it suggests an interpretable difference between models. If the ΔAIC is > 10, it suggests a strong difference between models, with the lower AIC value indicating the preferred model [81]. To also ascertain whether the relationship between LPC/LPOJ sulcal depth and cognition is specific to spatial orientation performance, or transferable to other general measures of cognitive processing, we investigated the generalizability of the sulcal-behavior relationship to another widely used measure of cognitive functioning: processing

speed [82]. Specifically, we used LooCV to predict processing speed instead of spatial orientation score. As with thickness, we compared the two models with the AIC.

Situating the slocs-v within modern group-level cortical parcellations

To putatively relate the slocs-v to modern multimodal (HCP multimodal parcellation, HCP-MMP [37]) and cytoarchitectural (Julich-Brain atlas [43]) regions of the cerebral cortex located in fsaverage template space, we quantified the Dice coefficient overlap between the slocs-v of each participant (resampled to fsaverage space) and the individual regions of interest comprising the HCP-MMP and Julich-Brain parcellations.

Retinotopic response mapping of LPC/LPOJ sulci

To assess whether any of the LPC/LPOJ sulci related to retinotopic representations, we leveraged population receptive field mapping data [46]. For each sulcal MPM (as the retinotopic data were only available in this template space), we extracted the mean R^2 values (i.e., the percentage of variance in each vertex explained by the population receptive field model) for vertices that showed meaningful retinotopic responses across participants (thresholded at $R^2 > 10\%$) [33].

Competing interests

The authors declare no competing financial interests.

Data availability

The processed data required to perform all statistical analyses and reproduce all Figures, as well as the probability maps, are available on GitHub (https://github.com/cnl-berkeley/stable_projects). Anonymized HCP neuroimaging data are publicly available on ConnectomeDB (db.humanconnectome.org). Raw data will be made available from the corresponding author upon request.

Code availability

The code is available on GitHub (https://github.com/cnl-berkeley/stable_projects) and Open Science Framework (https://osf.io/7fwqk/).

Acknowledgments

This research was supported by NSF CAREER Award 2042251 (PI Weiner). Neuroimaging and behavioral data were provided by the HCP, WU-Minn Consortium (PIs: David Van Essen and Kamil Ugurbil; NIH Grant 1U54-MH-091657) funded by the 16 NIH Institutes and Centers that support the NIH Blueprint for Neuroscience Research, and the McDonnell Center for Systems Neuroscience at Washington University. We thank Jacob Miller, Benjamin Parker, and Willa Voorhies for helping develop the analysis pipelines implemented in this project. We also thank the HCP researchers for participant recruitment and data collection and sharing, as well as the participants who participated in the study.

References

1. Amiez, C., Wilson, C. R. E. & Procyk, E. Variations of cingulate sulcal organization and link with cognitive performance. *Sci. Rep.* **8**, 1–13 (2018).
2. Amiez, C. *et al.* Sulcal organization in the medial frontal cortex provides insights into primate brain evolution. *Nat. Commun.* **10**, 1–14 (2019).
3. Cachia, A. *et al.* Towards Deciphering the Fetal Foundation of Normal Cognition and Cognitive Symptoms From Sulcation of the Cortex. *Front. Neuroanat.* **15**, 712862 (2021).
4. Garrison, J. R. *et al.* Paracingulate sulcus morphology is associated with hallucinations in the human brain. *Nat. Commun.* **6**, 8956 (2015).
5. Nakamura, M., Nestor, P. G. & Shenton, M. E. Orbitofrontal Sulcogyral Pattern as a Transdiagnostic Trait Marker of Early Neurodevelopment in the Social Brain. *Clin. EEG Neurosci.* **51**, 275–284 (2020).
6. Ammons, C. J. *et al.* The mid-fusiform sulcus in autism spectrum disorder: Establishing a novel anatomical landmark related to face processing. *Autism Res.* **14**, 53–64 (2021).
7. Fornito, A. *et al.* Individual differences in anterior cingulate/paracingulate morphology are related to executive functions in healthy males. *Cereb. Cortex* **14**, 424–431 (2004).
8. Lopez-Persem, A., Verhagen, L., Amiez, C., Petrides, M. & Sallet, J. The Human Ventromedial Prefrontal Cortex: Sulcal Morphology and Its Influence on Functional Organization. *J. Neurosci.* **39**, 3627–3639 (2019).
9. Harper, L. *et al.* Prenatal Gyrification Pattern Affects Age at Onset in Frontotemporal Dementia. *Cereb. Cortex* (2022) doi:10.1093/cercor/bhab457.
10. Weiner, K. S. The Mid-Fusiform Sulcus (sulcus sagittalis gyri fusiformis). *Anat. Rec.* **302**, 1491–1503 (2019).
11. Miller, J. A. *et al.* Sulcal morphology of ventral temporal cortex is shared between humans

and other hominoids. *Sci. Rep.* **10**, 17132 (2020).

12. Miller, J. A., Voorhies, W. I., Lurie, D. J., D'Esposito, M. & Weiner, K. S. Overlooked Tertiary Sulci Serve as a Meso-Scale Link between Microstructural and Functional Properties of Human Lateral Prefrontal Cortex. *J. Neurosci.* **41**, 2229–2244 (2021).
13. Willbrand, E. H. *et al.* Uncovering a tripartite landmark in posterior cingulate cortex. *Science Advances* **8**, eabn9516 (2022).
14. Hathaway, C. B. *et al.* Defining putative tertiary sulci in lateral prefrontal cortex in chimpanzees using human predictions. *Brain Struct. Funct.* (2023) doi:10.1007/s00429-023-02638-7.
15. Willbrand, E. H. *et al.* Sulcal morphology of posteromedial cortex substantially differs between humans and chimpanzees. *Communications Biology* **6**, 1–14 (2023).
16. Willbrand, E. H., Ferrer, E., Bunge, S. A. & Weiner, K. S. Development of human lateral prefrontal sulcal morphology and its relation to reasoning performance. *J. Neurosci.* (2023) doi:10.1523/JNEUROSCI.1745-22.2023.
17. Voorhies, W. I., Miller, J. A., Yao, J. K., Bunge, S. A. & Weiner, K. S. Cognitive insights from tertiary sulci in prefrontal cortex. *Nat. Commun.* **12**, 5122 (2021).
18. Yao, J. K., Voorhies, W. I., Miller, J. A., Bunge, S. A. & Weiner, K. S. Sulcal depth in prefrontal cortex: a novel predictor of working memory performance. *Cereb. Cortex* bhac173 (2022) doi:10.1093/cercor/bhac173.
19. Willbrand, E. H., Voorhies, W. I., Yao, J. K., Weiner, K. S. & Bunge, S. A. Presence or absence of a prefrontal sulcus is linked to reasoning performance during child development. *Brain Struct. Funct.* **227**, 2543–2551 (2022).
20. Parker, B. J. *et al.* Hominoid-specific sulcal variability is related to face perception ability. *Brain Struct. Funct.* (2023) doi:10.1007/s00429-023-02611-4.
21. Sanides, F. Structure and function of the human frontal lobe. *Neuropsychologia* **2**, 209–219

(1964).

22. Van Essen, D. C., Donahue, C. J. & Glasser, M. F. Development and Evolution of Cerebral and Cerebellar Cortex. *Brain Behav. Evol.* **91**, 158–169 (2018).
23. Zilles, K., Palomero-Gallagher, N. & Amunts, K. Development of cortical folding during evolution and ontogeny. *Trends Neurosci.* **36**, 275–284 (2013).
24. Petrides, M. *Atlas of the Morphology of the Human Cerebral Cortex on the Average MNI Brain*. (Academic Press, 2019).
25. Segal, E. & Petrides, M. The morphology and variability of the caudal rami of the superior temporal sulcus. *Eur. J. Neurosci.* **36**, 2035–2053 (2012).
26. Zlatkina, V. & Petrides, M. Morphological patterns of the intraparietal sulcus and the anterior intermediate parietal sulcus of Jensen in the human brain. *Proc. Biol. Sci.* **281**, (2014).
27. Drudik, K., Zlatkina, V. & Petrides, M. Morphological patterns and spatial probability maps of the superior parietal sulcus in the human brain. *Cereb. Cortex* (2022) doi:10.1093/cercor/bhac132.
28. Goodale, M. A. & Milner, A. D. Separate visual pathways for perception and action. *Trends Neurosci.* **15**, 20–25 (1992).
29. Humphreys, G. F. & Tibon, R. Dual-axes of functional organisation across lateral parietal cortex: the angular gyrus forms part of a multi-modal buffering system. *Brain Struct. Funct.* **228**, 341–352 (2023).
30. Harvey, B. M., Klein, B. P., Petridou, N. & Dumoulin, S. O. Topographic representation of numerosity in the human parietal cortex. *Science* **341**, 1123–1126 (2013).
31. Harvey, B. M., Fracasso, A., Petridou, N. & Dumoulin, S. O. Topographic representations of object size and relationships with numerosity reveal generalized quantity processing in human parietal cortex. *Proc. Natl. Acad. Sci. U. S. A.* **112**, 13525–13530 (2015).
32. Konen, C. S. & Kastner, S. Representation of eye movements and stimulus motion in

topographically organized areas of human posterior parietal cortex. *J. Neurosci.* **28**, 8361–8375 (2008).

33. Mackey, W. E., Winawer, J. & Curtis, C. E. Visual field map clusters in human frontoparietal cortex. *Elife* **6**, (2017).
34. Schurz, M., Tholen, M. G., Perner, J., Mars, R. B. & Sallet, J. Specifying the brain anatomy underlying temporo-parietal junction activations for theory of mind: A review using probabilistic atlases from different imaging modalities. *Hum. Brain Mapp.* **38**, 4788–4805 (2017).
35. Tomaiuolo, F. & Giordano, F. Cerebal sulci and gyri are intrinsic landmarks for brain navigation in individual subjects: an instrument to assist neurosurgeons in preserving cognitive function in brain tumour surgery (Commentary on Zlatkina et al.). *The European journal of neuroscience* vol. 43 1266–1267 (2016).
36. Tomaiuolo, F. *et al.* Sulci and gyri are topological cerebral landmarks in individual subjects: a study of brain navigation during tumour resection. *Eur. J. Neurosci.* **55**, 2037–2046 (2022).
37. Glasser, M. F. *et al.* A multi-modal parcellation of human cerebral cortex. *Nature* **536**, 171–178 (2016).
38. Vendetti, M. S. & Bunge, S. A. Evolutionary and developmental changes in the lateral frontoparietal network: a little goes a long way for higher-level cognition. *Neuron* **84**, 906–917 (2014).
39. Wendelken, C. Meta-analysis: how does posterior parietal cortex contribute to reasoning? *Front. Hum. Neurosci.* **8**, 1042 (2014).
40. Karnath, H. O. Spatial orientation and the representation of space with parietal lobe lesions. *Philos. Trans. R. Soc. Lond. B Biol. Sci.* **352**, 1411–1419 (1997).
41. Gur, R. C. *et al.* An fMRI study of sex differences in regional activation to a verbal and a

spatial task. *Brain Lang.* **74**, 157–170 (2000).

42. Kong, R. *et al.* Spatial Topography of Individual-Specific Cortical Networks Predicts Human Cognition, Personality, and Emotion. *Cereb. Cortex* **29**, 2533–2551 (2019).
43. Amunts, K., Mohlberg, H., Bludau, S. & Zilles, K. Julich-Brain: A 3D probabilistic atlas of the human brain's cytoarchitecture. *Science* **369**, 988–992 (2020).
44. Cunningham, D. J. *Contribution to the Surface Anatomy of the Cerebral Hemispheres*. (Academy House, 1892).
45. Wang, L., Mruczek, R. E. B., Arcaro, M. J. & Kastner, S. Probabilistic Maps of Visual Topography in Human Cortex. *Cereb. Cortex* **25**, 3911–3931 (2015).
46. Benson, N. C. *et al.* The Human Connectome Project 7 Tesla retinotopy dataset: Description and population receptive field analysis. *J. Vis.* **18**, 23 (2018).
47. Caspers, S. *et al.* Probabilistic fibre tract analysis of cytoarchitectonically defined human inferior parietal lobule areas reveals similarities to macaques. *Neuroimage* **58**, 362–380 (2011).
48. Wang, J. *et al.* Tractography-based parcellation of the human left inferior parietal lobule. *Neuroimage* **63**, 641–652 (2012).
49. Steel, A., Billings, M. M., Silson, E. H. & Robertson, C. E. A network linking scene perception and spatial memory systems in posterior cerebral cortex. *Nat. Commun.* **12**, 2632 (2021).
50. Reveley, C. *et al.* Superficial white matter fiber systems impede detection of long-range cortical connections in diffusion MR tractography. *Proc. Natl. Acad. Sci. U. S. A.* **112**, E2820–8 (2015).
51. Van Essen, D. C. *et al.* Mapping connections in humans and non-human primates. in *Diffusion MRI* 337–358 (Elsevier, 2014). doi:10.1016/b978-0-12-396460-1.00016-0.
52. Cottaar, M. *et al.* Modelling white matter in gyral blades as a continuous vector field.

Neuroimage **227**, 117693 (2021).

53. Schilling, K. *et al.* Confirmation of a gyral bias in diffusion MRI fiber tractography. *Hum. Brain Mapp.* **39**, 1449–1466 (2018).
54. Schilling, K. G. *et al.* Superficial white matter across development, young adulthood, and aging: volume, thickness, and relationship with cortical features. *Brain Struct. Funct.* **228**, 1019–1031 (2023).
55. Pron, A., Deruelle, C. & Coulon, O. U-shape short-range extrinsic connectivity organisation around the human central sulcus. *Brain Struct. Funct.* **226**, 179–193 (2021).
56. Bodin, C. *et al.* Plis de passage in the superior temporal sulcus: Morphology and local connectivity. *Neuroimage* **225**, 117513 (2021).
57. Connolly, C. J. *External morphology of the primate brain*. (CC Thomas, 1950).
58. Armstrong, E., Schleicher, A., Omran, H., Curtis, M. & Zilles, K. The ontogeny of human gyrification. *Cereb. Cortex* **5**, 56–63 (1995).
59. Régis, J. *et al.* 'Sulcal Root' Generic Model: a Hypothesis to Overcome the Variability of the Human Cortex Folding Patterns. *Neurol. Med. Chir.* **45**, 1–17 (2005).
60. Leroy, F. *et al.* New human-specific brain landmark: the depth asymmetry of superior temporal sulcus. *Proc. Natl. Acad. Sci. U. S. A.* **112**, 1208–1213 (2015).
61. Bodin, C., Takerkart, S., Belin, P. & Coulon, O. Anatomo-functional correspondence in the superior temporal sulcus. *Brain Struct. Funct.* **223**, 221–232 (2018).
62. Natu, V. S. *et al.* Sulcal Depth in the Medial Ventral Temporal Cortex Predicts the Location of a Place-Selective Region in Macaques, Children, and Adults. *Cereb. Cortex* **31**, 48–61 (2021).
63. Naselaris, T., Allen, E. & Kay, K. Extensive sampling for complete models of individual brains. *Current Opinion in Behavioral Sciences* **40**, 45–51 (2021).
64. Gratton, C., Nelson, S. M. & Gordon, E. M. Brain-behavior correlations: Two paths toward

reliability. *Neuron* vol. 110 1446–1449 (2022).

65. Rosenberg, M. D. & Finn, E. S. How to establish robust brain-behavior relationships without thousands of individuals. *Nature neuroscience* vol. 25 835–837 (2022).
66. Allen, E. J. *et al.* A massive 7T fMRI dataset to bridge cognitive neuroscience and artificial intelligence. *Nat. Neurosci.* **25**, 116–126 (2022).
67. Roell, M. *et al.* Sulcation of the intraparietal sulcus is related to symbolic but not non-symbolic number skills. *Dev. Cogn. Neurosci.* **51**, 100998 (2021).
68. Borne, L., Rivière, D., Mancip, M. & Mangin, J.-F. Automatic labeling of cortical sulci using patch- or CNN-based segmentation techniques combined with bottom-up geometric constraints. *Med. Image Anal.* **62**, 101651 (2020).
69. Lyu, I. *et al.* Labeling lateral prefrontal sulci using spherical data augmentation and context-aware training. *NeuroImage* vol. 229 117758 Preprint at https://doi.org/10.1016/j.neuroimage.2021.117758 (2021).
70. Dale, A. M., Fischl, B. & Sereno, M. I. Cortical surface-based analysis. I. Segmentation and surface reconstruction. *Neuroimage* **9**, 179–194 (1999).
71. Fischl, B., Sereno, M. I. & Dale, A. M. Cortical surface-based analysis. II: Inflation, flattening, and a surface-based coordinate system. *Neuroimage* **9**, 195–207 (1999).
72. Glasser, M. F. *et al.* The minimal preprocessing pipelines for the Human Connectome Project. *Neuroimage* **80**, 105–124 (2013).
73. Barch, D. M. *et al.* Function in the human connectome: task-fMRI and individual differences in behavior. *Neuroimage* **80**, 169–189 (2013).
74. Welker, W. Why Does Cerebral Cortex Fissure and Fold? in *Cerebral Cortex: Comparative Structure and Evolution of Cerebral Cortex, Part II* (eds. Jones, E. G. & Peters, A.) 3–136 (Springer US, 1990). doi:10.1007/978-1-4615-3824-0_1.
75. Chi, J. G., Dooling, E. C. & Gilles, F. H. Gyral development of the human brain. *Ann.*

Neurol. **1**, 86–93 (1977).

76. Glasser, M. F. & Van Essen, D. C. Mapping human cortical areas in vivo based on myelin content as revealed by T1- and T2-weighted MRI. *J. Neurosci.* **31**, 11597–11616 (2011).
77. Willbrand, E. H., Bunge, S. A. & Weiner, K. S. Neuroanatomical and functional dissociations between variably present anterior lateral prefrontal sulci. *bioRxiv* 2023.05.25.542301 (2023) doi:10.1101/2023.05.25.542301.
78. Heinze, G., Wallisch, C. & Dunkler, D. Variable selection - A review and recommendations for the practicing statistician. *Biom. J.* **60**, 431–449 (2018).
79. Dickerson, B. C. *et al.* Detection of cortical thickness correlates of cognitive performance: Reliability across MRI scan sessions, scanners, and field strengths. *Neuroimage* **39**, 10–18 (2008).
80. Gogtay, N. *et al.* Dynamic mapping of human cortical development during childhood through early adulthood. *Proc. Natl. Acad. Sci. U. S. A.* **101**, 8174–8179 (2004).
81. Wagenmakers, E.-J. & Farrell, S. AIC model selection using Akaike weights. *Psychon. Bull. Rev.* **11**, 192–196 (2004).
82. Kail, R. & Salthouse, T. A. Processing speed as a mental capacity. *Acta Psychol.* **86**, 199–225 (1994).